PHYSICAL REVIEW C

NUCLEAR PHYSICS

Volume 26 *Third Series* Number 4

OCTOBER 1982

Published by

THE AMERICAN PHYSICAL SOCIETY

through the

AMERICAN INSTITUTE OF PHYSICS

$^{14}N+^{13}C$ fusion cross sections and compound nucleus limitation in ^{27}Al

D. E. DiGregorio,* J. Gomez del Campo, Y. D. Chan,† J. L. C. Ford, Jr., and D. Shapira
Oak Ridge National Laboratory, Oak Ridge, Tennessee 37830

M. E. Ortiz
Instituto de Fisica, Universidad Nacional Autonoma de Mexico, Mexico 20, D.F.

(Received 4 June 1982)

Fusion cross sections for the $^{14}N+^{13}C$ system have been measured by detecting the evaporation residues at five bombarding energies which correspond to high excitation energies in the compound nucleus: $E^*(^{27}Al)=64-110$ MeV. The ^{27}Al nucleus can be populated by four different heavy-ion entrance channels—$^{15}N+^{12}C$, $^{16}O+^{11}B$, $^{14}N+^{13}C$, and $^{17}O+^{10}B$—which are accessible to experimental measurements. Comparing the present data with those already existing for the above channels, it is found that for $E^*>60$ MeV the curves E^* vs J_{cr} for each system converge, which may be indicative of a limitation imposed by the compound nucleus. The data are discussed in terms of existing models for entrance channel and statistical yrast line limitations. The highest energy point also suggests the existence of a maximum absolute angular momentum limit of $\sim 28\hbar$.

[NUCLEAR REACTIONS $^{14}N+^{13}C$ $E(^{14}N)=86.0$, 103.8, 149.0, 161.3, and 180.0 MeV; measured $d^2\sigma/d\Omega\,dE$ for reaction products from $Z=5$ to 12. Extracted σ_{fus}, σ_D, σ_R.]

I. INTRODUCTION

In the last few years a considerable effort has been made in the study of heavy ion fusion reactions, experimentally as well as theoretically. Fusion cross sections have been measured for a large number of systems. From these measurements, it was well established that fusion excitation functions for light heavy ions show clearly three different regimes[1]: at lower energies (region I) the fusion cross section σ_{fus} is rather close to the total reaction cross section σ_R, and the penetration of the Coulomb and centrifugal barriers is the mechanism governing the order of magnitude of σ_{fus}; at higher energies (region II) σ_{fus} decreases substantially below σ_R, owing to the onset of the dynamical competition between fusion and direct reactions. A third energy regime (region III) has been observed in a few systems[2] at very high energies where the σ_{fus} drops proportionally to $1/E_{c.m.}$. This behavior has been attributed to the limitation of fusion arising from rotational properties of the compound nucleus such as the liquid drop limit.[3]

By systematically examining the measurements performed in the mass region

$$A_1+A_2 \leq A_{CN}=80\ ,$$

it seems clear that the fusion cross section at low energies (region I) is governed primarily by entrance channel effects. However, the behavior of σ_{fus} in region II is not yet clearly understood. Several explanations have been presented in order to describe this intermediate energy regime. All these approaches generally fall into two categories—those which rely on the properties of the projectile and the target (entrance channel models) and those which emphasize the properties of the compound nucleus. Among the former models, that of Glas and Mosel[4] has been quite successful in describing the fusion cross section, especially the low energy regime and the prediction of the bend in σ_{fus}. Although the parameters R_B (the interaction barrier radius) and $V(R_B)$ (the interaction barrier) extracted from the experimental data follow a clear trend making possible the applicability of the model, the values extracted for the critical radius R_{cr} and the potential at R_{cr}, $V(R_{cr})$, do not show a systematic trend.

In searching for alternative explanations to describe the behavior of σ_{fus} at high energies, several attempts have been reported recently[5,6] pos-

tulating that the structure of the compound nucleus plays a dominant role in the limitations observed; generally, these limitations are discussed in terms of the critical angular momentum l_{cr} which can lead to fusion. With increasing bombarding energy $E_{c.m.}$ the entrance channel may bring in an angular momentum larger than the compound nucleus can support (the yrast spin at the corresponding excitation energy E^*), and therefore the compound nucleus cannot be formed. The question of whether the compound nucleus is the limiting factor would be answered by the location of the yrast line. However, the problem is that the yrast lines are not known empirically for the relevant angular momentum range for fusion in the light systems ($A_{CN} \leq 60$). Motivated by this fact, Diebel *et al.*[7] performed calculations based on the cranked deformed shell model to obtain yrast lines in the mass region from $A=24-60$. Their calculations for the nuclei ^{26}Al and ^{24}Mg have clearly shown that fusion reactions do not populate, and therefore are not limited by, the yrast line because this always lies below the experimental fusion band. Recently, it was suggested that a heavy ion system, in order to fuse, must reach an effective yrast line in which the compound nucleus has a sufficient level density. Using different approaches, models have been proposed by Lee *et al.*[6] and by Vandenbosh and Lazzarini[5] to calculate the statistical yrast line relevant for fusion. In the model of Lee *et al.*,[6] it is assumed that the statistical yrast line lies parallel to the usual yrast line, with a shift in energy ΔQ_{CN} and a slope determined by a rigid-body moment of inertia $\mathcal{I}_{rig}$. Vandenbosh and Lazzarini[5] define the statistical yrast line using the criterion that the average width of compound nucleus levels Γ_J divided by the average spacing of a particular angular momentum D_J is the order of unity.

In order to determine which mechanism, either the entrance channel effects or the compound nucleus properties, imposed the more restrictive limit to fusion, one has to study different entrance channels populating the same compound nucleus. In this sense, the ^{27}Al nucleus is unique among the light systems because it can be populated by four different heavy-ion entrance channels which are readily accessible to experimental measurements. These channels [$^{15}N+^{12}C$ ($Q_{CN}=17.2$ MeV), $^{16}O+^{11}B$ ($Q_{CN}=21.1$ MeV), $^{14}N+^{13}C$ ($Q_{CN}=23.2$ MeV), and $^{17}O+^{10}B$ ($Q_{CN}=28.4$ MeV)] provide a large data set to test the various theoretical models for fusion, particularly those related to the Q_{CN} value dependence and compound nucleus limitations. Although fusion cross sections for all these systems have been measured by the Saclay[8] and Argonne[9] groups at the excitation energy range in ^{27}Al below 60 MeV, little information is yet available at higher energies in the region which is most relevant to the above-mentioned models and limitations. Recently, we reported measurements at higher energies involving the $^{17}O+^{10}B$ and $^{15}N+^{12}C$ systems.[10,11] The intent of this article is to present fusion cross sections extracted for the $^{14}N+^{13}C$ system at five bombarding energies covering the range of excitation energy in ^{27}Al $E^*=64-110$ MeV. In Sec. II, we discuss the experimental technique which was used. The analysis of the data and the results are described in Sec. III. In Sec. IV, the fusion cross sections extracted are discussed in terms of the existing models.

II. EXPERIMENTAL TECHNIQUE

Measurements were performed at the Oak Ridge Isochronous Cyclotron using beams of ^{14}N to bombard self-supporting isotopically enriched (99%) ^{13}C targets at five different bombarding energies: $E_{^{14}N}=86.0$, 103.8, 149.0, 161.3, and 180.0 MeV. The thickness of ^{13}C foils (57 and 125 $\mu g/cm^2$) was determined by measuring the energy loss of α particles (provided by a calibrated ^{244}Cm source) in the material. A thin deposit of gold (1 $\mu g/cm^2$) had been evaporated on the ^{13}C target for normalization purposes. Cross sections were extracted by detecting the evaporation residues resulting from the compound nucleus formation and subsequent particle evaporation. The identification of the reaction products with $Z=4$ to 12 were made by measuring the energy loss ΔE and total energy E in a conventional ΔE-E detector consisting of a position-sensitive solid-state detector for the E element and an ionization chamber for the ΔE counter. This counter telescope enabled the detection of nine angles simultaneously in one-degree steps with a total solid angle of 3 msr. In addition, two solid state ΔE-E telescopes, both employing a 10 μm ΔE and a 2000 μm E counter, were used at small scattering angles (4° and 9°). Angular distributions were measured for the range of laboratory angles from 4° to 35°. Data were stored on disc in a large three-dimensional array (ΔE vs E vs position) for the position-sensitive telescope and in two-dimensional arrays (ΔE vs E) for the other two E-ΔE counters.

Absolute normalization was determined by Rutherford scattering of ^{14}N from Au at E_{lab} (^{14}N)=86 MeV together with the measured ^{13}C to Au target thickness. This procedure provides an accurate measurement of the detector angles ($\sim 0.1°$) and es-

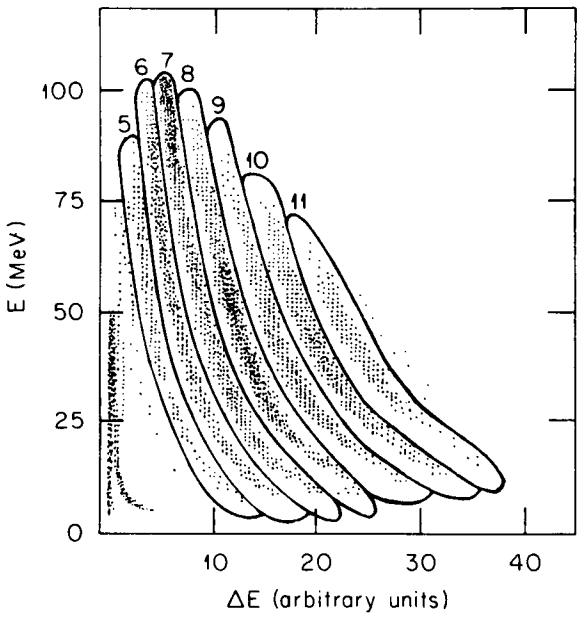

FIG. 1. A ΔE vs E array for the reaction products of the $^{14}N + ^{13}C$ system at $E(^{14}N) = 103.8$ MeV and $\theta_{lab} = 12.2°$. The total energy E was obtained by analog summation of the signals from the ionization chamber and solid state detector. The curves around the contour of constant Z were used to obtain projections along the E axis.

tablishes an uncertainty in the absolute cross section estimated to be of the order of $\sim 5\%$. However, other uncertainties also contribute to the total error in the cross section, such as counting statistics, extrapolation of the angular distribution to angles less than 4° and greater than 35°, and the identification of the evaporation residues. In our measurements, the statistical uncertainties are negligible ($< 1\%$) and the uncertainties arising from the extrapolation procedure are estimated to be $< 2\%$. The most important source of error in the fusion cross section arises from the identification of evaporation residues due to their strong overlap with the peripheral reaction components, especially when the fusion products have masses comparable to or less than that of the projectile. In the fusion cross sections reported in this paper, the absolute errors are estimated to be 9%.

III. ANALYSIS OF THE DATA AND RESULTS

A representative two-dimensional E-ΔE spectrum, measured at $E_{lab}(^{14}N) = 103.8$ MeV and a laboratory angle of 12.2°, is shown in Fig. 1. The various reaction products are clearly well-resolved from $Z = 4$ to $Z = 11$. The curves around the contours of constant Z were used to extract projections along the E axis, which represents the total energy obtained by analog summation of the signals from the ionization chamber and the solid state detector. Typical examples of the energy distributions $(d^2\sigma/d\Omega\, dE)$ for several reaction products are

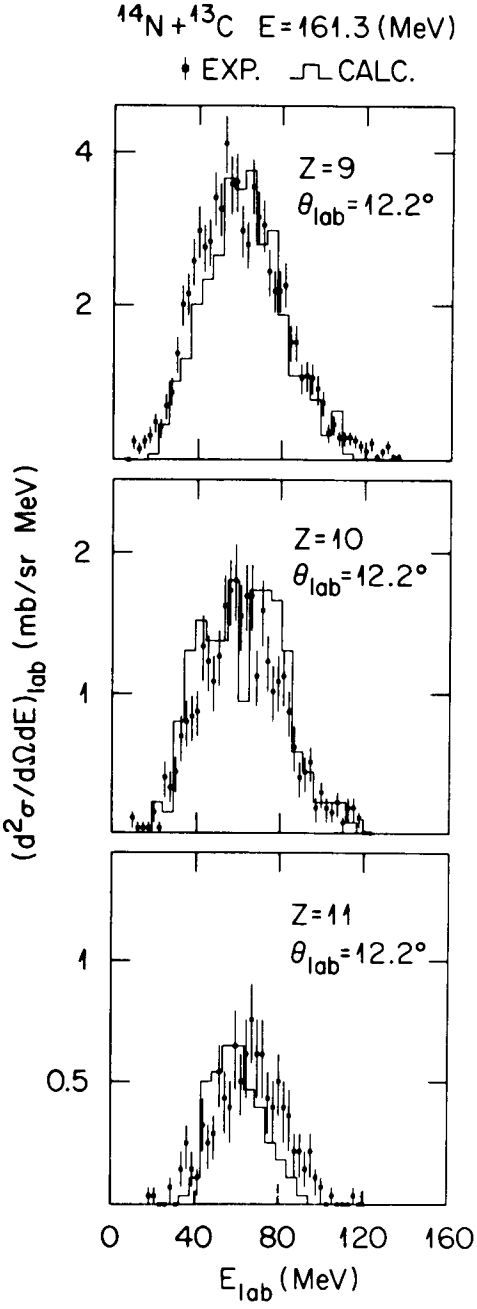

FIG. 2. Energy spectra of reaction products of $Z = 9$ to $Z = 11$ for the $^{14}N + ^{13}C$ system at $E(^{14}N) = 161.3$ MeV and $\theta_{lab} = 12.2°$. The histograms are the results of Monte Carlo calculations of the energy spectra of the evaporation residues of a fully equilibrated ^{27}Al compound nucleus.

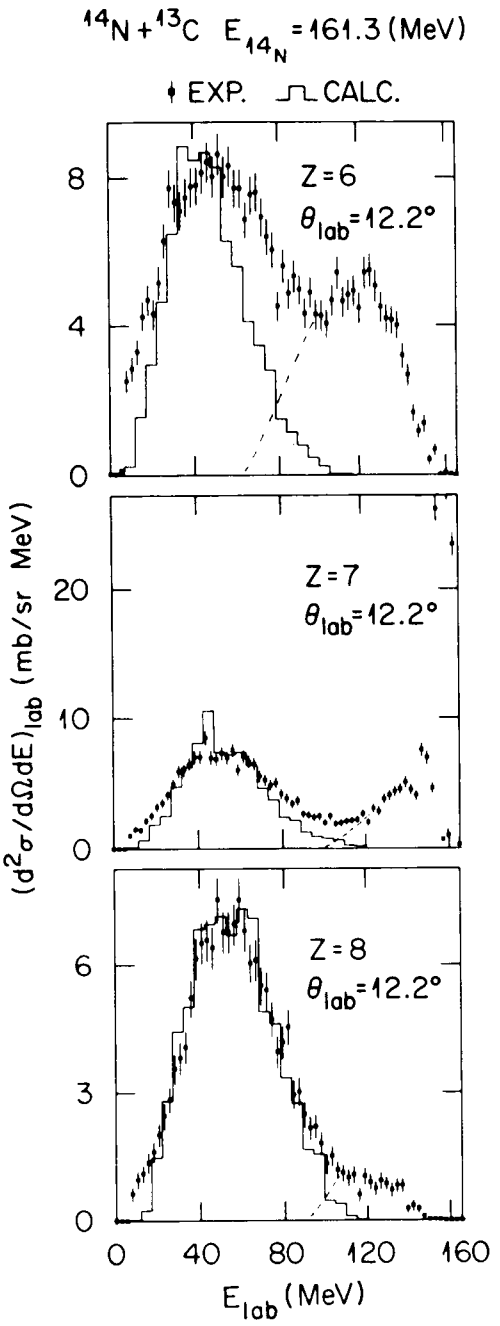

FIG. 3. Energy spectra of reaction products of $Z=6$ to $Z=8$ for the $^{14}N + ^{13}C$ system at $E(^{14}N)=161.3$ MeV and $\theta_{lab}=12.2°$. The histograms have the same meaning as in Fig. 2. The dashed lines indicate the deconvolution procedure used to separate the evaporation residues (lower energy group) from the peripheral reaction component (higher energy group).

shown in Figs. 2 and 3. The shape (centroid and width) of these spectra can be understood in terms of simple kinematic arguments.[12] For example, the yields of fluorine, neon, and sodium nuclei (shown in Fig. 2) are characteristic of residues of compound nucleus formation followed by evaporation of light particles.

The energy distribution of the evaporation residues exhibit centroids (E_{ER}) which are localized around the average kinetic energy of the compound nucleus

$$E_{CN}=(M_{proj}/M_{CN})E_{proj},$$

where M_{proj} and E_{proj} are the mass and laboratory energy of the projectile, respectively. The centroids E_{ER} are given approximately by

$$E_{ER}\simeq(M_{ER}/M_{CN})E_{CN}\cos^2\theta_{lab},$$

where M_{ER} is the mass of the evaporation residue, and the width of the energy distribution gets broadened by the recoil imparted by the light particle emission. Energy spectra corresponding to oxygen, nitrogen, and carbon (Fig. 3) nuclei contain, in addition to the evaporation residue compound, contributions from peripheral two-body reactions. These components have centroids E_{DI}, whose velocity is typical of the projectile, and are given approximately by

$$E_{DI}\simeq(M_{DI}/M_{proj})E_{proj},$$

where M_{DI} is the mass of the fragments produced by the peripheral process. In these cases, spectrum deconvolution is necessary to separate out the fusing and the direct reaction components. To illustrate kinematic effects on the evaporation residues, it is convenient to transform the measured energy spectrum $d^2\sigma/d\Omega\,dE$ into a velocity distribution $V_R{}^{-2}d^2\sigma/d\Omega\,dV_R$, where V_R is the velocity of the evaporation residue, in a way similar to that of Ref. 2. For a complete momentum transfer and equilibrium decay the centroids of the velocity distributions are given by $V_{CN}\cos\theta_L$, where V_{CN} is the compound nucleus velocity and θ_L is the laboratory angle. Since Z, but not A, was identified in the present experiment, the mass used to transfer the energy spectrum into a velocity distribution was that given by Monte Carlo calculations. The uncertainties in these procedures are usually less than 5% since the mass spread for a given Z is not very large (only 2 to 3 mass units). Figure 4 shows the velocity distributions for the case of $^{14}N + ^{13}C$ at $E(^{14}N)=161.3$ MeV, $\theta_{lab}=12.2°$ and reaction products from $Z=6$ to 11. The line labeled $V_{CN}\cos\theta_L$ corresponds to the expected centroid of evaporation residues coming from a fully equilibrated compound nucleus. The fact that the lower velocity groups peak near the $V_{CN}\cos\theta_L$ line is a strong indication of complete fussion and equilibrium decay.

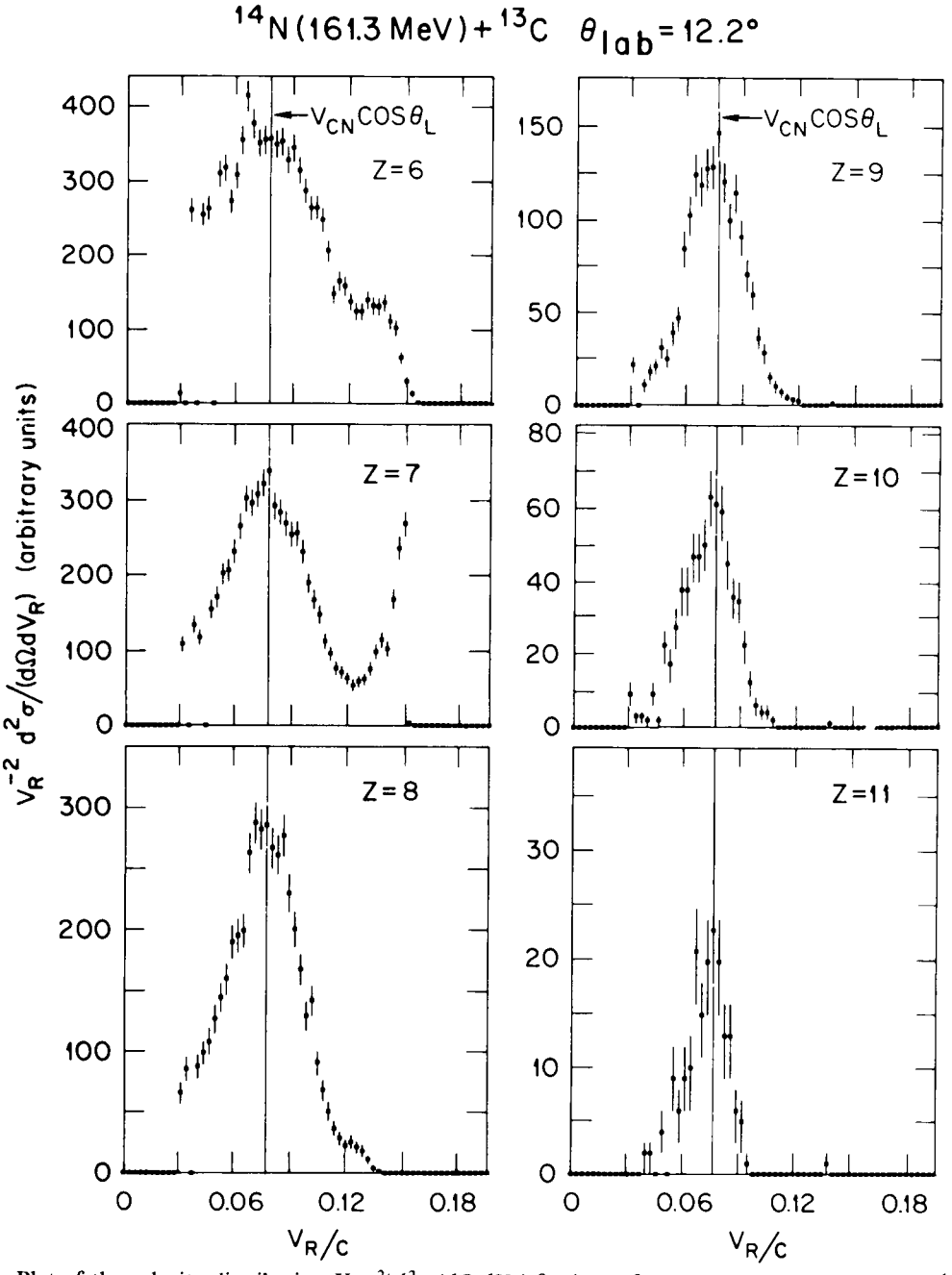

FIG. 4. Plot of the velocity distribution $V_R{}^{-2}(d^2\sigma/d\Omega\, dV_R)$ for ions of $Z=6$ to 11, produced by the $^{14}N + {}^{13}C$ reaction at $E(^{14}N)=161.3$ MeV. The horizontal scale gives the velocity of the evaporation residue V_R in terms of the speed of light c. The vertical line indicates the expected centroid ($V_{CN}\cos\theta_L$) for complete fusion and equilibrium decay.

TABLE I. Evaporation residue cross sections measured at five bombarding energies for the $^{14}N + {}^{13}C$ system.

E_{lab} (MeV)	σ_Z (mb)							
	$Z=5$	$Z=6$	$Z=7$	$Z=8$	$Z=9$	$Z=10$	$Z=11$	$Z=12$
86.0		51	165	328	153	228	117	34
103.8	33	124	221	321	145	140	69	10
149.0	87	314	257	193	90	56	21	3
161.3	138	314	232	168	80	45	14	
180.0	119	278	186	133	59	30	15	

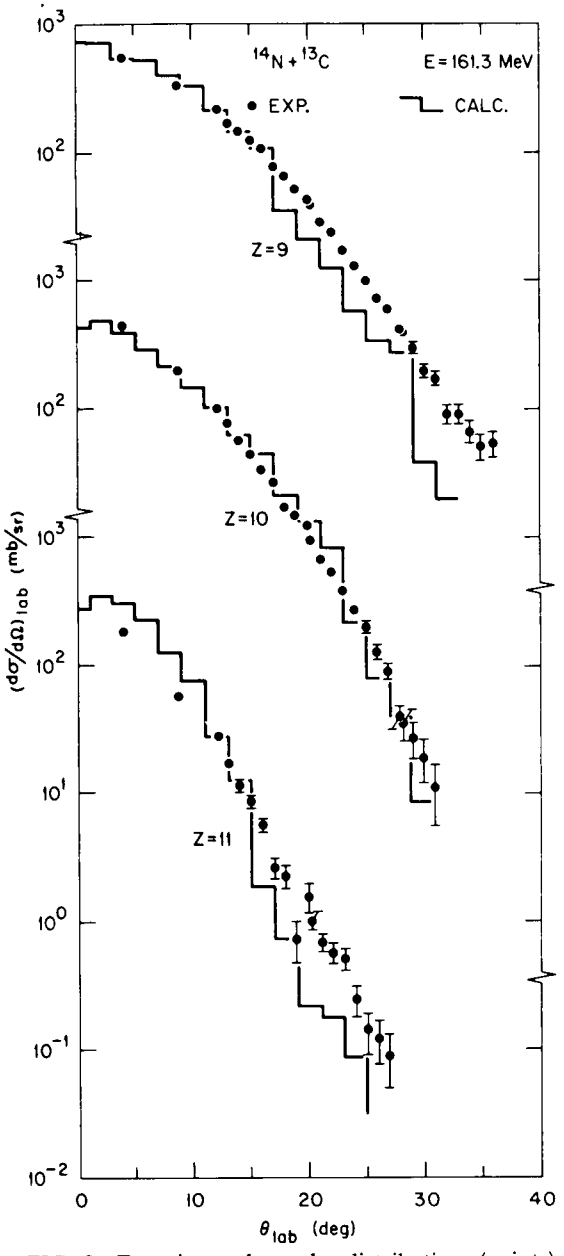

FIG. 5. Experimental angular distributions (points) of evaporation residues of $Z=9$ to 11 for the $^{14}N + ^{13}C$ reaction at $E(^{14}N)=161.3$ MeV. The histograms are the results of the Monte Carlo calculations using the code LILITA.

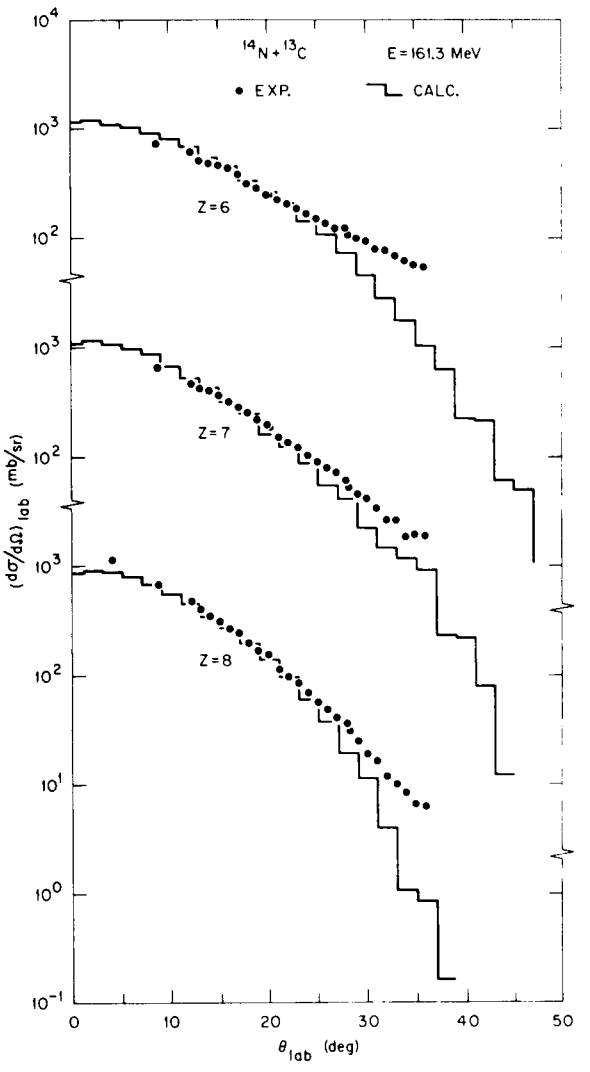

FIG. 6. Experimental angular distributions (points) of evaporation residues of $Z=6$ to 8 for the $^{14}N + ^{13}C$ reaction at $E(^{14}N)=161.3$ MeV. The histograms are the results of the Monte Carlo calculations using the code LILITA.

By integrating the energy spectra measured at each angle, one can obtain angular distributions for the fusion component for each atomic number for the five bombarding energies. Angular distributions for evaporation residues with $Z=6-11$ at $E_{lab}(^{14}N)=161.3$ MeV are illustrated in Figs. 5 and 6. Inspection shows that the angular distributions become more widely spread in angle as more mass is evaporated. The contributions of each atomic number to the fusion cross section are obtained by integration of the angular distributions, such as those shown in Figs. 5 and 6. These results are presented in Table I which shows the contribution σ_Z (in mb) of the evaporation residue components for ions from $Z=5$ to $Z=12$ at five bombarding energies—86.0, 103.8, 149.0, 161.3, and 180.0 MeV. The total fusion cross sections were obtained by summing the individual contribution of each evaporation residue σ_Z. The results are summarized in Table II. Columns 1, 2, and 3 give the laboratory bombarding energy E_{lab}, the center-of-mass energy $E_{c.m.}$, and the excitation energy E^* in the compound nucleus, respectively. Column 4 shows the fusion cross section σ_{fus} (in mb). Because of the

TABLE II. Summary of experimental results for $^{14}N + {}^{13}C$ in the present measurement.

E_{lab} (MeV)	$E_{c.m.}$ (MeV)	E^*_{CN} (MeV)	σ_{fus} (mb)	J_{cr} ($\hbar$)
86.0	41.4	64.6	1076±95	20.4±1.0
103.8	50.0	73.2	1063±95	22.4±1.0
149.0	71.7	94.9	1043±95	26.7±1.3
161.3	77.7	100.9	1042±95	27.8±1.3
180.0	86.7	109.9	924±85	27.7±1.3

fact that the yields of residues with $Z < 5$ cannot be clearly separated (using the method described above) from those due to other mechanisms, their contributions to σ_{fus} were estimated by employing statistical model calculations. Hence, the measured fusion cross sections for 149.0, 161.3, and 180.0 MeV were increased by the amounts of 2%, 5%, and 11%, respectively.

Even though the fusion and the direct reaction components could be properly identified using simple kinematical arguments, it is more convenient to perform statistical model calculations in order to give credence to our analysis of the evaporation residues. We have used the Monte Carlo evaporation code LILITA[13] to obtain laboratory energy spectra, angular distributions, and relative yields of the evaporation products.

In Figs. 2 and 3 the histograms show the results of the statistical model calculations for the energy distributions of residues with $Z = 6-11$. The agreement with the data exhibited here indicates the reliability of the identification of the evaporation residues and of the deconvolution procedure for separating out the direct reaction components. Also the calculated angular distributions (histograms) shown in Figs. 5 and 6 reproduce the experimental data (full dots) well. Both the predicted energy and angular distributions have been arbitrarily normalized to the data to enable a better shape comparison. In Fig. 7 the relative yields of the evaporation residues, expressed as a percentage of the total fusion cross section extracted from the measurements, are compared with those yields predicted by the Hauser-Feshbach Monte Carlo calculations at five different bombarding energies. The reasonable agreement, for a wide energy range $E_{lab} = 86.0-180.0$ MeV, between the observed and predicted yields suggests the formation of a compound nucleus in statistical equilibrium.

IV. DIRECT-REACTION COMPONENTS AND TOTAL REACTION CROSS SECTION

As shown in Fig. 5, the energy distributions of oxygen, nitrogen, and carbon ions exhibit a double-peaked shape: one peak at low energies, typical of the evaporation residues, and the other at higher energies with a centroid characteristic of the velocity of the projectile. The dashed lines in the figure indicate the way both components (fusion and direct reaction) were unfolded. The latter component contains contributions of the two-body reactions in which one or more nucleons are either transferred or are emitted by the projectile after having been excited in a peripheral colhsion. Similarly, as for the fusion components, these high energy components can be integrated over energy and angle to obtain the direct reaction cross sections. Table III shows the contributions to the total direct cross sections of ions from $Z = 5$ to $Z = 8$ at the five bombarding energies measured. Providing there has been no double-counting of fragments, and that no reaction products have been lost, for example, through detector thresholds, then the sum of the fusion cross section σ_{fus} and the direct reaction cross section σ_D should give the total reaction cross section σ_R. In Table IV, the results for σ_{fus}, σ_D, and σ_R at the five bombarding energies are summarized. By fitting the elastic scattering data using the optical model one can obtain the total reaction cross section σ_R (OM). Parameters used in the calculations are also given in Table IV. Since complete elastic scattering data exist at two bombarding energies, 103.8 and 161.3 MeV, we performed the optical model analysis keeping all the parameters fixed except the depth of the imaginary potential W_I, which was varied until the best fit was obtained at these two energies. For the other bombarding energies the deduced energy dependent W_I was used. Reasonably good agreement was found between the experimental total reaction cross section and that predicted by the optical model.

V. DISCUSSION

The question remains as to whether the entrance channel properties or the structure of the compound nucleus plays the dominant role in the observed limitations of σ_{fus} at high energies. Therefore, we will discuss our present results in the $^{14}N + {}^{13}C$ sysfem

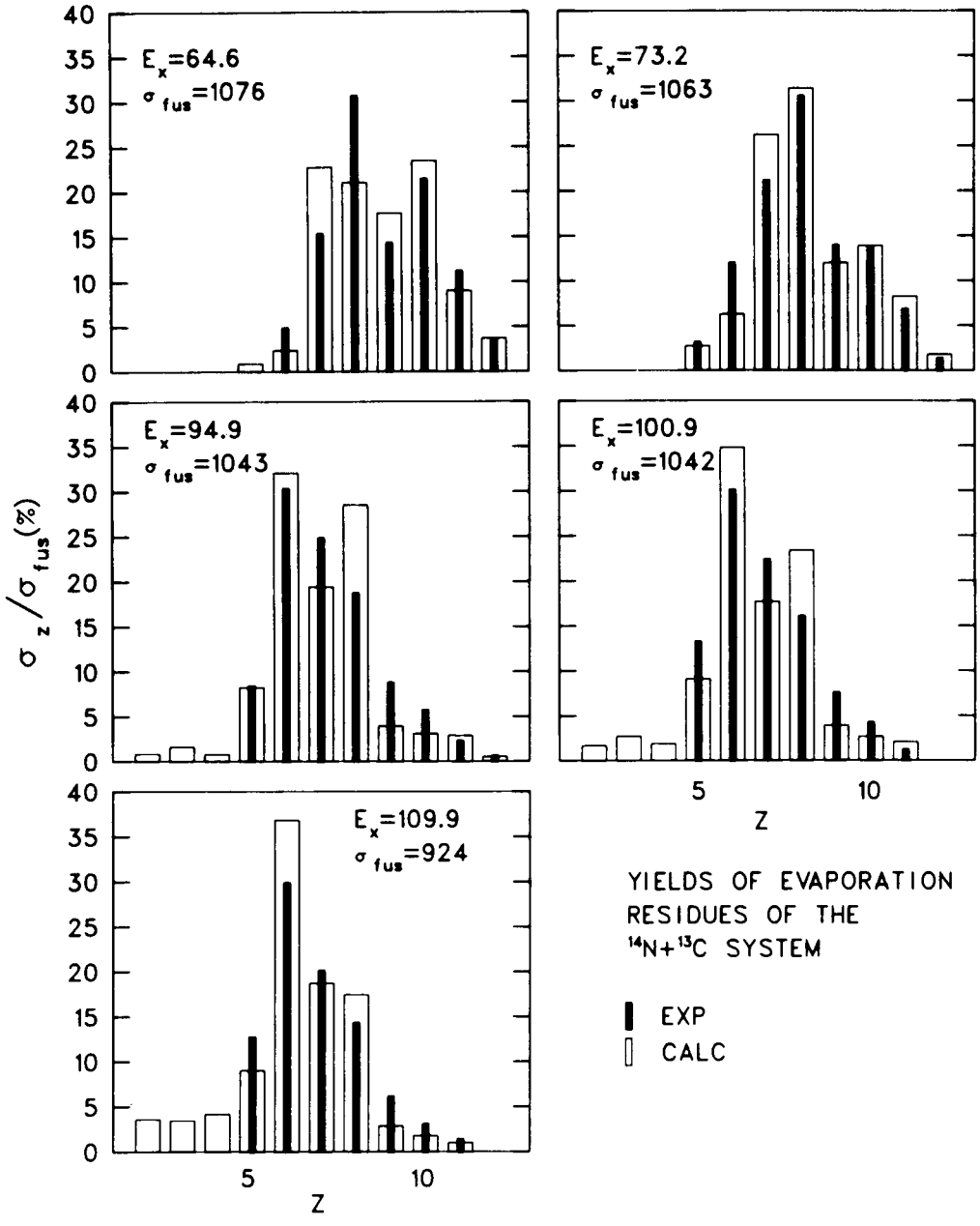

FIG. 7. Experimental (solid bars) and theoretical (histograms) evaporation yields, plotted as a percentage of σ_{fus}. The comparison between experiment and calculations is shown for each of the five bombarding energies observed in the present experiment. The calculations were done with the Monte Carlo code LILITA.

TABLE III. Direct-reaction cross sections σ_D for the $^{14}N + ^{13}C$ system.

E_{Lab} (MeV)	Z 5	6	7	8	σ_D (mb)
86.0	76	135	158	8	377±35
103.8	85	175	123	35	418±40
149.0	115	125	111	31	382±35
161.3	98	158	127	38	421±40
180.0	115	169	131	34	449±40

TABLE IV. Summary of cross section measurements for $^{14}N + {}^{13}C$ system.

E_{lab} (MeV)	$E_{c.m.}$ (MeV)	σ_{fus} (mb)	σ_D (mb)	σ_R (mb)	σ_R (OM)[a] (mb)
86.0	41.4	1076	377	1453	1344
103.8	50.0	1063	418	1481	1365
149.0	71.7	1043	382	1425	1392
161.3	77.7	1042	421	1463	1398
180.0	86.7	924	449	1373	1404

[a]Optical model parameters: The real part was fixed for all energies to be $V_R = 21.74$ MeV, $r_R = 1.25$ fm, and $a_R = 0.52$ fm. The geometry of the imaginary potential was taken to be $r_I = 1.22$ fm, $a_I = 0.54$ fm, and its strength $W_I = 6.05 + 0.083 E_{c.m.}$.

at $E_{c.m.} = 41 - 87$ MeV together with existing experimental data for the same system at low energies ($E_{c.m.} = 15 - 30$ MeV) and for the related channels $^{17}O + {}^{10}B$, $^{11}B + {}^{16}O$, and $^{12}C + {}^{15}N$ taken from the literature.[8-11]

Frequently, the fusion cross sections are discussed in terms of the classical expression

$$\sigma_{fus}(E_{c.m.}) = \pi R^2 \left[1 - \frac{V(R)}{E_{c.m.}}\right], \tag{1}$$

where the radius R is given by

$$R = r(A_1^{1/3} + A_2^{1/3}),$$

and r is a parameter which depends on the energy region. The Glas and Mosel model[4] combined this energy dependence with the concept of quantum mechanical penetration of the interaction barrier $V_B(R_B)$ at low energies, and the criterion that the two colliding nuclei must reach a critical distance R_{cr} in order to fuse at high energies. In this framework, the fusion cross section as a function of the center-of-mass energy can be expressed as

$$\sigma_{fus}(E_{c.m.}) = \pi \lambda^2 \sum_{l=0}^{l_{cr}} (2l+1)\{1 + \exp[2\pi(V_{Bl} - E_{c.m.})/\hbar\omega]^{-1}\}, \tag{2}$$

where l_{cr}, the critical angular momentum, is given by

$$l_{cr}(l_{cr}+1) = 2\mu R_{cr}^2/\hbar^2 (E_{c.m.} - V_{cr}) \tag{3}$$

and V_{Bl} is given by

$$V_{Bl} = V_B + \hbar^2 l(l+1)/2\mu R_B^2, \tag{4}$$

where $R_{cr}(R_B)$ and $V_{cr}(V_B)$ are the critical (barrier) radii and potential strengths, and μ is the reduced mass in the entrance channel. The result of fitting Eq. (1) to the experimental points using the parameters $r_{cr} = 1.18$ fm, $V_{cr} = -1.4$ MeV, $r_B = 1.45$ fm, $V_B = 6.7$ MeV, and $\hbar\omega = 2.0$ MeV, is shown in Fig. 8 as a solid curve drawn through the data points.

An important feature shown in Fig. 8 is the fall-off of σ_{fus} at the highest energy measured. The dashed line intersecting the origin gives the expected trend of σ_{fus} vs $1/E_{c.m.}$ for a constant maximum angular momentum of $\sim 27.8\hbar$. This would indicate the saturation of the angular momentum with increasing energy. It seems reasonable to associate this angular momentum limit with asymptotic properties of the compound nucleus; hence, it can be taken as evidence in favor of a liquid-drop limit

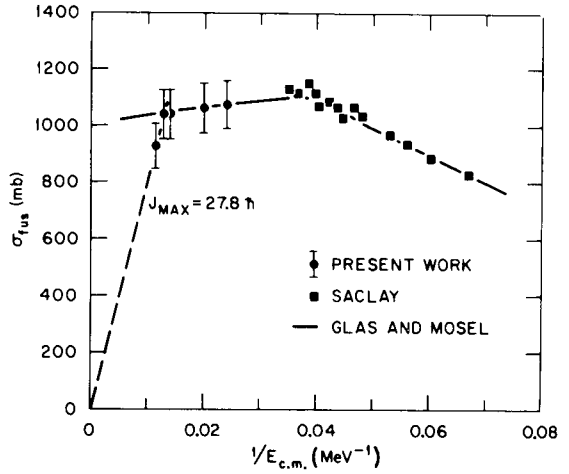

FIG. 8. The fusion cross section σ_{fus} for the $^{14}N + {}^{13}C$ system, plotted versus the inverse of the center-of-mass energy $E_{c.m.}$. The circles are the present measurements and the squares are those of Ref. 8. The solid line through the experimental points is the result of the Glas-Mosel fit with parameters given in Table V. The dashed line intersecting the origin indicates that $\sigma_{fus} \alpha 1/E_{c.m.}$ at high energies, consistent with an absolute angular momentum limit of $\sim 27.8\hbar$.

effect as was found in ^{26}Al (Ref. 2) and ^{24}Mg.[14] The value of $27.8\hbar$ agrees with the value predicted by the rotating liquid drop model of Ref. 3.

Another convenient way to study limitations on fusion is to transform the measured $\sigma_{fus}(E_{c.m.})$ data into a completely equivalent representation $E^*(l_{cr})$ by using the well known expression for the fusion cross section in the sharp cutoff approximation,

$$\sigma_{fus}=\pi\lambda^2(l_{cr}+1)^2 , \quad (5)$$

and the relation

$$E^*=E_{c.m.}+Q , \quad (6)$$

where l_{cr} is the critical angular momentum in the entrance channel and Q is the separation energy. In the $E^*(l_{cr})$ representation the experimental fusion data form separate bands for each entrance channel which populates the same compound nucleus. The ^{27}Al nucleus has been studied in the past through the different experimentally accessible channels: $^{16}O+^{11}B$, $^{14}N+^{13}C$, $^{12}C+^{15}N$, and $^{17}O+^{10}B$ at low energy ($E_{c.m.}\leq 30$ MeV) (Refs. 8 and 9) and, more recently, measurements in the latter two systems have been reported at higher energies.[10,11] In Fig. 9, all the available experimental data together with the results of the present measurements are displayed. Glas-Mosel model calculations have been also performed for each individual entrance channel to fit the experimental data. The parameters extracted in the fitting procedure are given in Table V and the results of the calculations are plotted in Fig. 9.

Included in Table V for comparison are the Glas-Mosel parameters for $^{10}B+^{14}N$ (Ref. 14), $^{10}B+^{16}O$ (Ref. 2), and $^{14}N+^{12}C$.[2] As can be seen, the values of r_{cr} and V_{cr} do not follow any systematic trend. This behavior indicates that the fusion cross section at high energies shows drastic changes with respect to the addition or removal of nucleons from target or projectile and should be taken as evidence for the strong influence of microscopic structure in the fusion process.

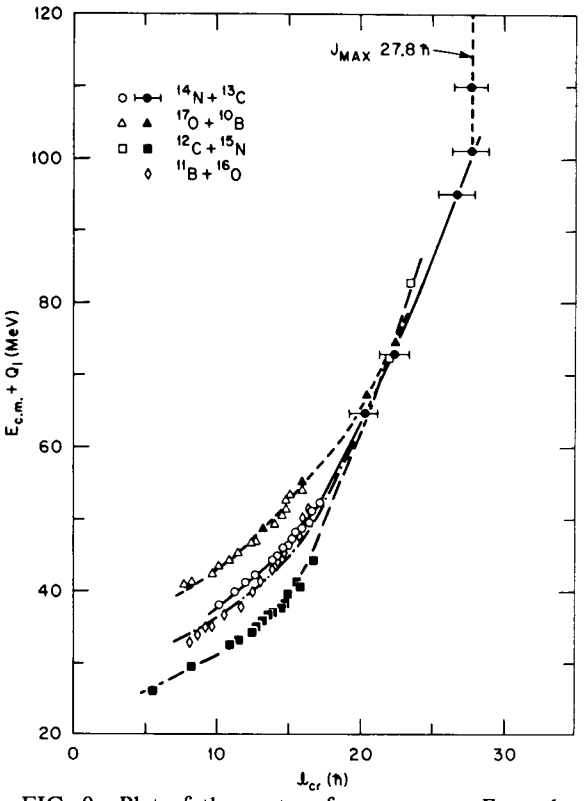

FIG. 9. Plot of the center-of-mass energy $E_{c.m.}$ plus separation energy Q_i versus the critical angular momentum (l_{cr}) deduced from the fusion cross section. Data points are shown for $^{14}N+^{13}C$, $^{15}N+^{12}C$, $^{10}B+^{17}O$, and $^{11}B+^{16}O$ measurements. The open circles, diamonds, and triangles are measurements of the Saclay group (Ref. 8) and the solid squares are those of the Argonne group (Ref. 9). Closed circles and triangles, and open squares are the present measurements and those of Refs. 10 and 11, respectively. The lines through the data points correspond to the Glas-Mosel fits with the parameters given in Table V.

From the comparison of the different fusion bands that populate the ^{27}Al compound nucleus

TABLE V. List of parameters used in the Glas and Mosel model calculations.

Channel	r_B (fm)[a]	V_B (MeV)[a]	r_{cr} (fm)[b]	V_{cr} (MeV)[b]	$\hbar\omega$ (MeV)
$^{10}B+^{17}O$	1.50	6.7	1.28	0.0	2.0
$^{13}C+^{14}N$	1.45	6.7	1.18	−1.4	2.0
$^{11}B+^{16}O$	1.50	7.7	1.20	0.0	2.0
$^{12}C+^{15}N$	1.53	6.7	1.05	−8.3	2.0
$^{10}B+^{16}O$	1.50	6.7	1.35	2.5	2.0
$^{12}C+^{14}N$	1.50	6.7	1.11	−1.9	2.0
$^{10}B+^{14}N$	1.50	6.8	1.17	−1.9	2.0

[a]Values deduced from low-energy measurements given in Refs. 2, 8, 9, and 14.
[b]Values deduced from the high-energy measurements of this work and those in Refs. 2, 8, 10, 11, and 14.

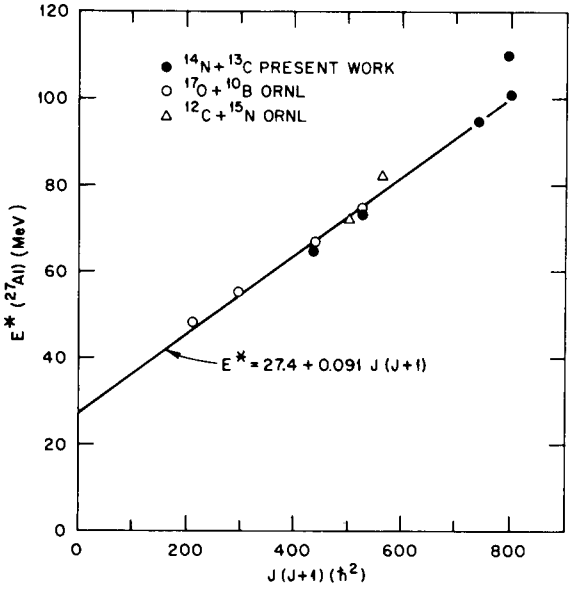

FIG. 10. Plot of the excitation energy in ^{27}Al vs $J(J+1)$. The value of the compound nucleus angular momentum J is extracted from the fusion measurements using the sharp cutoff approximation, i.e., $\sigma_{fus}=\pi\lambda^2(J+1)^2$. Data points are shown for $^{14}N+^{13}C$ (present measurements), $^{15}N+^{12}C$ (Ref. 11), and $^{10}B+^{17}O$ (Ref. 10). The solid line is the least squares fit of $E^*=E_0+\hbar^2/2\mathcal{I}J(J+1)$ to the data with extracted values of $E_0=27.4$ MeV and $\mathcal{I}/\hbar^2=5.5$ MeV^{-1}.

shown in Fig. 9, two different energy regimes seem to be well defined. For excitation energies below 60 MeV, the fusion bands are parallel and displaced by the differences in the separation energies, Q_i, of each channel. Quantum mechanical penetration of the interaction barrier is the dominant effect. Also, the barrier parameters r_B and V_B are very similar (see Table V). A completely analogous behavior of the fusion cross sections at low energies has been reported recently for the $^{10}B+^{13}C$ and $^{11}B+^{12}C$ systems.[15] The limitations imposed by Q values can be an extremely important factor, as was demonstrated in the comparison of the $^{14}N+^{10}B$ and $^{12}C+^{12}C$ systems.[14]

The unique feature of the data shown in Fig. 9 is that above 60 MeV of excitation all the fusion bands converge to a single line, and therefore the limitation on the fusion cross section appears to be dependent on the compound nucleus properties. In the study of $^{10}B+^{17}O$ (Ref. 10), suggestions were made to explain this effect in terms of the statistical yrast line treatment of Lee *et al.*[6] and Vandenbosch and Lazzarini,[5] although, as in the case of Glas-Mosel fits, the extracted parameters that fit the data are quite different for every channel. Using the model of Lee *et al.*[6] to fit the data given in Fig. 9, we extract values of $\Delta Q=25$ MeV and $r_0=1.45$ fm which are quite different from the values of 10 MeV and 1.20 fm suggested in Ref. 6. Also, using the model of Vandenbosch and Lazzarini requires the values of $r_0=1.45$ fm and $\Gamma/D=500$, rather than the suggested values[5] of $r_0=1.16$ and $\Gamma/D=1$.

To further illustrate the limitation imposed by the compound nucleus, the data obtained at Oak Ridge National Laboratory for the $^{14}N+^{13}C$ (present measurements), $^{15}N+^{12}C$ (Ref. 11), and $^{17}O+^{10}B$ (Ref. 10) systems are shown in Fig. 10 in an E^* vs $J(J+1)$ plot. The solid line through the data points is a least squares fit of

$$E^*=E_0+(\hbar^2/2\mathcal{I})J(J+1)\ ,$$

where the bandhead $E_0=27.4$ MeV and $\mathcal{I}/\hbar^2=5.5$ MeV^{-1}. It is important to point out that the value of $\mathcal{I}/\hbar^2$ extracted from the fusion data is essentially the same as that obtained by the coherence width analysis of the $^{12}C(^{15}N,\alpha)$ reaction data at lower energies,[16] indicating that, indeed, the extracted moment of inertia is that of the compound nucleus ^{27}Al.

VI. SUMMARY

The $^{14}N+^{13}C$ system has been studied at five bombarding energies from 6 to 13 MeV/nucleon. The fusion and peripheral cross sections were extracted and their sum agrees well with the total reaction cross section predicted by the optical model. The dominant mechanism leading to evaporation-residuelike events is that of complete fusion and equilibrium decay, even at 13 MeV/nucleon. The study of the fusion of $^{14}N+^{13}C$ at high energies together with the existing data for $^{10}B+^{17}O$, $^{12}C+^{15}N$, and $^{11}B+^{16}O$ shows that in the E^* vs J plot the fusion bands converge to a common trajectory, indicating that the limitation on the fusion is imposed by the compound nucleus. Nevertheless, the extracted effective yrast line for fusion deviates quite significantly from predictions of current models. At the highest energy studied, a saturation of the angular momentum is found at $J_{max}=27.8\hbar$.

ACKNOWLEDGMENTS

One of us (D.E.D.G.) gratefully acknowledges the hospitality and support of the Physics Division at the Oak Ridge National Laboratory during his stay. This work was supported by the Oak Ridge National Laboratory, operated by Union Carbide Corporation under contract W-7405-eng-26 with the U. S. Department of Energy.

*Present address: Comisión Nacional de Energía Atómica, 1429 Buenos Aires, Argentina.

†Present address: Nuclear Science Division, Lawrence Berkeley Laboratory, Berkeley, CA 94720.

[1]U. Mosel, Comments Nucl. Part. Phys. 9, 213 (1981).

[2]J. Gomez del Campo, R. A. Dayras, J. A. Biggerstaff, D. Shapira, A. H. Snell, P. H. Stelson, and R. G. Stokstad, Phys. Rev. Lett. 43, 26 (1979).

[3]S. Cohen, F. Plasil, and W. J. Swiatecki, Ann. Phys. (N.Y.) 82, 557 (1974).

[4]D. Glas and U. Mosel, Nucl. Phys. A237, 429 (1975).

[5]R. Vandenbosch and J. Lazzarini, Phys. Rev. C 23, 1074 (1980).

[6]S. M. Lee, T. Matsuse, and A. Arima, Phys. Rev. Lett. 45, 165 (1980).

[7]M. Diebel, D. Glas, U. Mosel, and H. Chandra, Nucl. Phys. A333, 253 (1980).

[8]J. P. Wieleczko, S. Harar, M. Conjeaud, and F. Saint-Laurent, Phys. Lett. 93B, 35 (1980); S. Harar and J. P. Wieleczko, lecture presented at the International School of Poiana, Brasov, Romania, 1980.

[9]D. G. Kovar, D. F. Geesaman, T. H. Braid, Y. Eisen, W. Henning, T. R. Ophel, M. Paul, K. E. Rehm, S. J. Sanders, S. Sperr, J. P. Schiffer, S. L. Tabor, S. Vigdor, B. Zeidman, and F. W. Prosser, Jr., Phys. Rev. C 20, 1305 (1979).

[10]Y-d. Chan, D. E. DiGregorio, J. L. C. Ford, Jr., J. Gomez del Campo, M. E. Ortiz, and D. Shapira, Phys. Rev. C 25, 1410 (1982).

[11]R. Novotny, D. Shapira, Y-d. Chan, D. E. DiGregorio, J. L. C. Ford, J. Gomez del Campo, M. E. Ortiz, P. H. Stelson, and F. Pougheon Phys. Rev. C (to be published).

[12]J. Gomez del Campo, R. G. Stokstad, J. A. Biggerstaff, R. A. Dayras, A. H. Snell, and P. H. Stelson, Phys. Rev. C 19, 2170 (1979).

[13]J. Gomez del Campo and R. G. Stokstad, Oak Ridge National Laboratory Report ORNL-TM-7295, 1981.

[14]M. E. Ortiz, J. Gomez del Campo, Y-d. Chan, D. E. DiGregorio, J. L. C. Ford, Jr., D. Shapira, R. G. Stokstad, J. P. F. Sellschop, R. W. Parks, and D. Weiser, Phys. Rev. C 25, 1436 (1982).

[15]J. F. Mateja, A. D. Frawley, L. C. Dennis, K. Abdo, and K. W. Kemper, Phys. Rev. Lett. 47, 311 (1981).

[16]J. Gomez del Campo, J. L. C. Ford, Jr., R. L. Robinson, M. E. Ortiz, A. Dacal, and E. Andrade, Nucl. Phys. A297, 125 (1978).

PHYSICAL REVIEW C

Postmaster: If undeliverable, send notice on Form 3579 to:

American Institute of Physics
335 East 45th Street
New York, N.Y. 10017

SECOND CLASS POSTAGE PAID AT WOODBURY, N.Y. AND ADDITIONAL MAILING OFFICES

For editorial and subscription correspondence, please see inside front cover

ISSN: 0556-2813

THIRD SERIES, VOLUME 26, NUMBER 4 *CONTENTS* OCTOBER 1982

Nuclear Reactions

Heavy Ions

Fission

(Continued)